Geoscience Letters

RESEARCH LETTER

Effect of mesoscale eddies on the transport of low-salinity water from the Bay of Bengal into the Arabian Sea during winter

Jiechao Zhu[1,2], Yuhong Zhang[1,2,3*], Xuhua Cheng[4], Xiangpeng Wang[1,2], Qiwei Sun[1,3] and Yan Du[1,2,3]

Abstract

The distribution of sea surface salinity (SSS) in the Arabian Sea (AS) and Bay of Bengal (BoB) is in contrast due to differences in air-sea freshwater fluxes and river runoff inputs. The monsoon-induced inter-basin water exchange plays an important role in regional salinity balance and atmosphere–ocean feedback in the North Indian Ocean. The satellite SSS data set reveals that significant intraseasonal variability of SSS occurs in the region south of the Indian Peninsula with the strongest amplitude in winter. A case study in autumn-winter of 2016 showed that the Northeast Monsoon Current (NMC) and mesoscale eddies play a dominant role in the intraseasonal variability of the SSS in the region south of the Indian peninsula. In November, the East India Coastal Current (EICC) transports the low-salinity water southward to the region east of Sri Lanka. Meanwhile, a cyclonic eddy develops and moves westward south of the NMC. Both NMC and the cyclonic eddy advects the low-salinity water westward to the region south of the Indian Peninsula. Then, an anticyclonic eddy generates in the north of the NMC. Thus, an eddy pair forms for more than one and a half months, which develops and propagates westward, transporting low-salinity water westward. The perturbation of mesoscale eddies and SSS difference between BoB and AS leads to the significant intraseasonal variability of SSS.

Keywords: Sea surface salinity, Intraseasonal variability, Mesoscale eddies, North Indian Ocean

Introduction

The ocean salinity is not only an indicator of the global water cycle (Durack et al. 2012) but also determines the ocean density together with temperature, leading to the vertical stratification of the ocean and thermohaline circulation (Murtugudde and Busalacchi 1998; Vinogradova et al. 2019). Therefore, it plays a key part in the thermodynamic processes of the ocean. In recent years, the dynamic and thermodynamic processes of the North Indian Ocean and their responses to climate change have gained much more attention.

The sea surface salinity (SSS) in the North Indian Ocean has a large east–west contrast. Indian Peninsula divides the North Indian Ocean into two semi-closed basins, the Arabian Sea (AS) in the west and the Bay of Bengal (BoB) in the east. Although the AS and the BoB are at the same latitude and both affected by the monsoon, the salinity of the upper ocean is significantly different (Schott and McCreary 2001). The salinity of the AS is relatively high due to the ocean surface loss of freshwater with the annual evaporation exceeding precipitation as well as the influence of high-salinity water mass from the Red Sea and the Persian Gulf (Zhang et al. 2020). In the BoB, the annual mean precipitation and freshwater input by the rivers are abundant due to strong moisture flux convergence by the Southwest Monsoon (Schott et al. 2009), which causes the relatively low SSS (Vinayachandran et al., 2002). Especially in the estuary area, the SSS is lower than 25 psu in summer, far below the average salinity of the world ocean. In the equatorial Indian Ocean, a significant SSS

*Correspondence: zhangyuhong@scsio.ac.cn
[1] State Key Laboratory of Tropical Oceanography, South China Sea Institute of Oceanology, Chinese Academy of Sciences, Guangzhou 510301, China
Full list of author information is available at the end of the article

Zhu *et al. Geoscience Letters* (2022) 9:37

Page 2 of 14

gradient appears from west to east caused by increasing precipitation and water masses from adjacent areas (Schott and McCreary 2001).

Climatologically, the pattern of SSS in the northern Indian Ocean is generally consistent with evaporation minus precipitation (E–P). To maintain the long-term salt balance, the monsoon currents play an important role in the water mass exchange between the west and the east(Shetye et al. 1996; Durand et al. 2009). Using the synthetic site data, Rao and Sivakumar (2002) found that the seasonal variation of SSS in the North Indian Ocean is mainly determined by freshwater input and redistribution of high- and low-salinity water caused by ocean currents. The seasonally reversed monsoon current system in the North Indian Ocean dominates the water exchange between the AS and the BoB (Schott and McCreary 2001; Shankar et al. 2002; Schott et al. 2009; Zhang and Du 2012). The SSS distribution is strongly affected by horizontal advection on the seasonal cycle.

As part of the monsoonal current system, the East India Coastal Current (EICC) connects the north BoB with the south region and the equatorial Indian Ocean. Before and during the onset of the summer monsoon, EICC transports the high-salinity water from the AS and the equator to the northern BoB. From November to December and March to April, it flows southward and forms a continuous flow between the northern BoB and the southeast coast of Sri Lanka (Schott and McCreary, 2001; Vinayachandran et al. 2005). EICC effectively transports low-salinity water from the northern BoB to the region south of the Indian Peninsula, becoming a low-salinity water source for inter-basin transport.

The reversal monsoon current region south of the Indian Peninsula promotes the water exchange between the AS and the BoB, maintaining the salinity balance (Rao and Sivakumar 2002; Zhang and Du 2012). In summer, the Southwest Monsoon Current (SMC) carries the high-salinity waters from the AS into the BoB from the central. At the same time, the SSS in the northern BoB decreased significantly under the influence of considerable river runoff. These results demonstrated that river runoff is the dominant factor for the variation of SSS in the north BoB during the Southwest Monsoon (Howden and Murtuggude 2001; Han and McCreary 2001; Yu and McCreary 2004; Srivastava et al. 2020). In winter, the Northeast Monsoon Current (NMC) transports the low-salinity water carried by EICC from BoB to the west and imports it into the southeastern AS (Shenoi et al. 2005; Kurian and Vinayachandran 2007; Durand et al. 2007). Recently, observations from surface drifters and Argo floats suggest that the low-salinity water outflow from the BoB, westward into the south of Sri Lanka and eventually into the AS, is discontinuous (Hormann et al. 2019).

Hence, considering seasonal current only cannot reveal the essential dynamics of salinity transport.

Previous studies pointed out that the oceanic dynamic process in the North Indian Ocean has obvious intraseasonal signals. Sea surface height exhibits an evident intraseasonal cycle in the east of Sri Lanka and the adjacent regions, which is mainly related to eddy activities (Cheng et al. 2017). Greaser et al. (2020) pointed out that the number and amplitude of eddy in the BoB are closely related to the atmospheric Intraseasonal Variability (ISV) in the region. Affected by Madden–Julian Oscillation (MJO) or Intraseasonal Oscillation (ISO), the changes of SSS in the BoB have three distinct periods, 30–90 days, 10–20 days, and 3–7 days (Trott et al. 2019; Subrahmanyam et al. 2020).

This paper focuses on the role of eddies in low-salinity water transport region south of the Indian Peninsula during winter. Previous studies have pointed out that the SSS data from satellite observation such as Soil Moisture and Ocean Salinity (SMOS), Soil Moisture Active Passive (SMAP), and Aquarius can well capture the low-salinity water signature. Satellite SSS data sets suggested that eddies in the Eastern Tropical Pacific trap and advect water westward, which is associated with the intraseasonal variability of SSS with a leading timescale of 50–180 days (Hasson et al., 2019). In addition, eddy-induced northward salt flux was thought to be responsible for the lowest SSS maximum in the south Indian Ocean compared with the other two southern subtropical oceans (Qu et al. 2019). This paper uses the SMAP SSS data combined with other observation data to explore the role of eddies in water exchange between the BoB and the AS during wintertime.

Data and methods
Data
The SMAP satellite of the National Aeronautics and Space Administration (NASA) is designed to measure soil moisture and SSS (Fore et al. 2016). The SSS data of SMAP are obtained by sensors operating at 1.4 GHz in the L band, with a clipping width of about 1000 km. The SSS product used in this paper is JPL SMAP Level 3 CAP Sea Surface Salinity Standard Mapped Image 8-Day Running Mean V5.0 Validated Data set with 0.25° horizontal resolution, provided by Jet Propulsion Laboratory (JPL). The starting date for this data set is May 4, 2015. The time frame for the data used in this paper is from May 4, 2015, to Feb 29, 2020. The climatological SSS from World Ocean Atlas 2018 (WOA18) with a 1° horizontal resolution is used in this study. The data set is from the National Oceanographic Data Center (NCEI) of the United States and the World Data Service (WDS) of Maryland (Garcia et al., 2019). The climatological mixed layer

Zhu *et al. Geoscience Letters*   (2022) 9:37

Page 3 of 14

depth data with a 0.25° horizontal resolution is also from the WOA18.

The Argo project has been in operation for nearly 20 years and has about 4000 floats that provide continuous observations of ocean temperature, salinity, and pressure from the surface to 2000 dbar. The Argo data used in this paper were obtained from the Coriolis Argo Global Data Assembly Centre, with float numbers 2902153 and 2901896, at sampling intervals ranging from 5 to 10 days, and at maximum depths of about 2000 m.

The sea surface current data are obtained from the Ocean Surface Current Analysis Real-time (OSCAR) products, with a horizontal resolution of 1/3° (Bonjean and Lagerloef 2002) and have been uniformly interpolated into a 1/4° grid to calculate the salinity budget with the SMAP SSS. OSCAR products use satellite sea surface height, wind, and temperature to calculate global ocean currents directly. Sea Level Anomaly (SLA) data are provided by Copernicus Climate Change Service (C3S), which is obtained by removing the 20-year average from 1993 to 2012.

The daily accumulated evaporation and precipitation data are from the European Centre for Medium-Range Weather Forecasts (ECMWF). The daily accumulated data are calculated according to the ERA5 data, and the horizontal resolution of the data is 1/4°.

Salinity budget analysis

Following Rao and Sivakumar (2003) and Nyadjro et al. (2012), the mixed layer salinity evolution equation is expressed as follows:

$$\frac{\partial S}{\partial t} = \frac{(E-P)S}{h} - \left(U\frac{\partial S}{\partial x} + V\frac{\partial S}{\partial y} \right) - \frac{W_e \Delta S}{h} + D$$

where S is the averaged salinity of the mixed layer. The SSS is used in this paper to replace the averaged salinity of the mixed layer due to the relatively homogeneous salinity distribution within the mixed layer for the research region. E and P represent evaporation and precipitation, respectively. h is the mixed layer depth. U and V are zonal and meridional velocities, respectively. W_e is the vertical entrainment velocity. ΔS equals the bottom salinity of the mixed layer minus the average salinity in the mixed layer. From left to right, the first term represents the salinity tendency, the second term represents the forcing of freshwater flux, the third term represents the horizontal advection, and the fourth represents the vertical entrainment process. Previous studies have shown that the vertical entrainment is one order of magnitude smaller than the horizontal advection in the open ocean on the monthly mean state (Rao and Sivakumar 2003). In the upwelling area of the ocean, the effect of

vertical entrainment on salinity change is enhanced, but the contribution is still small (Kohler et al. 2018). Therefore, this paper only discusses the role of freshwater flux and horizontal advection. D represents the residual term, which contains errors caused by small-scale processes, such as vertical entrainment, diffusion, and mixing.

Results

Seasonal distribution of SSS in the North Indian Ocean and the role of ocean circulation

In the annual mean state, the East–West SSS differs largely in the North Indian Ocean (Fig. 1a). The salinity at the northern AS is close to 37 psu due to the freshwater flux with evaporation exceeding precipitation. The SSS with a value larger than 36 psu is throughout the basin, except in the Southeastern AS. In the BoB, the SSS gradually decreases toward the northern bay, forming an obvious salinity gradient. At the northernmost end, due to the large input of river runoff, the annual average SSS is below 30 psu (Fig. 1a). There is an obvious coastal low-salinity tongue that extends from the BoB to southeastern AS. South of it, especially along the equator, a high-salinity tongue extends from the west to the east, and then enters the BoB in the central parts (Fig. 1a). The distribution of high- and low-salinity tongues indicates the water exchanges between the two basins.

Previous studies suggested that the SMC in summer and NMC in winter play an essential role in water mass exchange between the two basins (Rao and Sivakumar 2002; Jenson 2003; Zhang and Du 2012). Besides, high-resolution SSS shows the patchy distribution of high- and low-salinity water in the region south of the Indian Peninsula and along the coastal region, indicating the contribution of eddies.

The seasonal water mass exchange between the AS and the BoB and the associated ocean processes can be shown in the seasonal climatologies of the SSS and SLA (Fig. 1b, c). During the winter, the SLA in south India shows a sharp gradient northward, accompanied by the westward extension of low-salinity waters into the South AS. The strongest gradient occurs near 5°N, corresponding to the main axis of NMC. The closed contours of the SLA suggest that mesoscale eddies may occur on both sides of the NMC with anticyclones in the north and cyclones in the south (Fig. 1b). In summer, the situation is almost opposite to that of winter, but the eddies are weak and easterly, mainly located to the south of the BoB (Fig. 1c). In addition, eddy processes are also evident along the western coast of the BoB, which may have a strong influence on the water mass exchange between the BoB and the AS (Babu et al. 1991). An anticyclonic eddy is located in the southeastern AS, which is named Lakshadweep high (LH) (Bruce
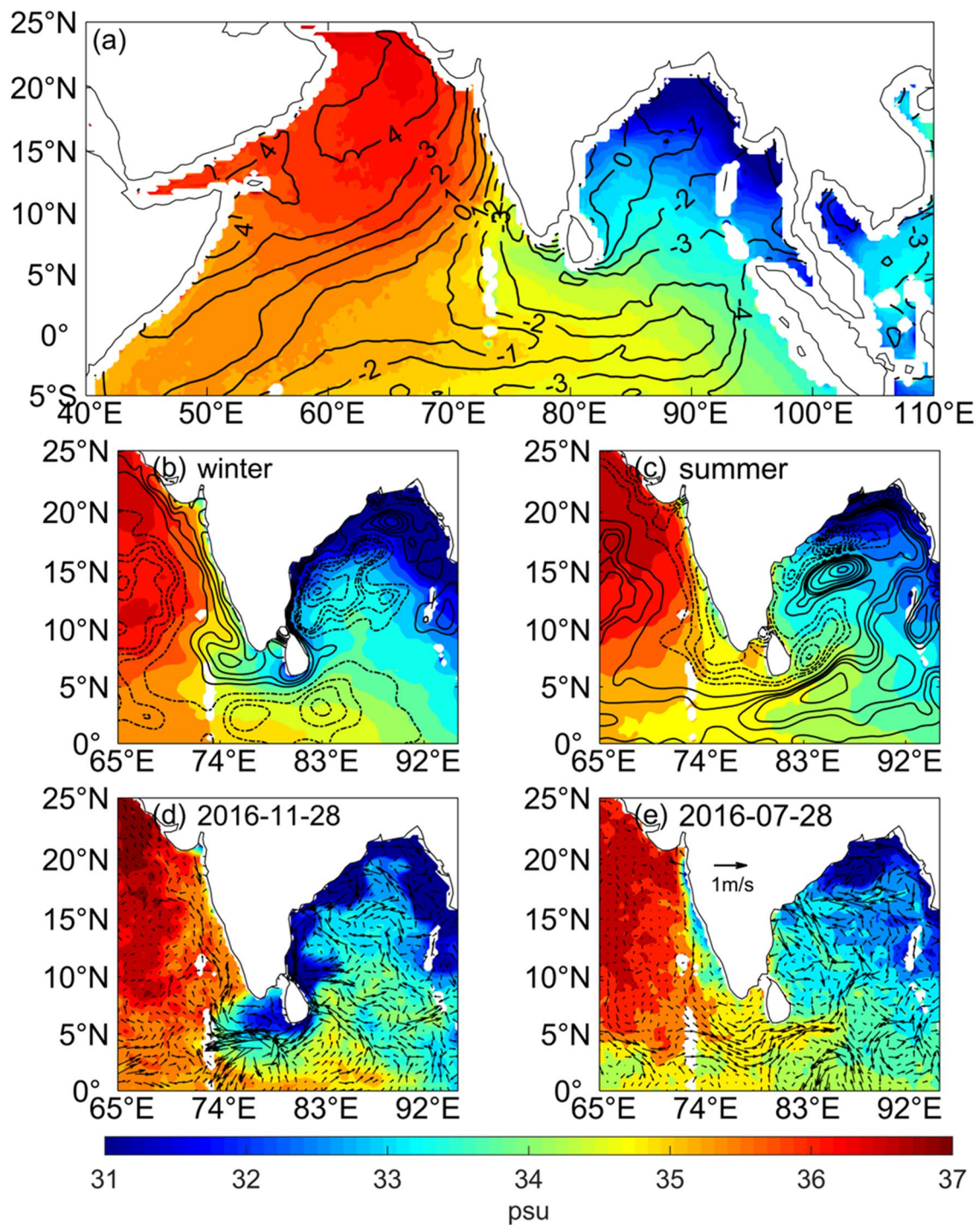
Fig. 1 Annual mean distribution of SSS in the North Indian Ocean and the inter-basin water transport in winter and summer, respectively. **a** Annual mean of SSS (shading, psu) and E minus P(contour lines, mm). **b** The five-year average winter SSS (shading, psu) and SLA (contours). **c** The five-year average summer SSS (shading, psu) and SLA (contour lines). The contour interval is 0.02 m with a span from − 0.10 to 0.14 m. The regional mean SLA in the northern Indian Ocean (0.004m) is subtracted. **d** SSS (shading, psu) and sea surface current (vector, m / s) on Nov 28, 2016, and **e** same as d but for Jul 28, 2016

et al. 1994). Noticeable low-salinity water can be seen in the LH, indicating its important role in the low-salinity advection into the AS.

The 8-day running mean SSS and 5-day mean current show that a large amount of the low-salinity water with SSS lower than 32 psu was advected to the region south of the Indian Peninsula on November 28, 2016 (Fig. 1d). These low-salinity water can be traced back to the northern BoB, which is advected southward by the EICC (Fig. 1d). In the region south of the Indian Peninsula, an eddy pair with anticyclone north and cyclone south occurred near 78°E. A large amount of low-salinity water was trapped in the anticyclone and some were advected to the western region by the edge-jet of the eddy-pair (Fig. 1d). In summer, the low-salinity water region south of the Indian Peninsula is replaced by the high-salinity water with SSS higher than 35 psu, nearly 3 psu saltier than that in winter (Figs. 1d, e). The corresponding eastward SMC occurs region south of the Indian Peninsula and advects the high-salinity water from the AS into the BoB in the central region. The mesoscale eddies can also be noticed during the transport of high-salinity water on July 28, 2016, but their influence is mainly confined to the southern BoB (Fig. 1e).

Intraseasonal variability of SSS in the region south of the Indian Peninsula and the related ocean dynamics

The root mean square (RMS) of SSS in WOA18 climatology and SMAP SSS daily data show that the variability of the daily SSS is much stronger than in seasonal climatology. Indeed, they show similar patterns in the north Indian Ocean (Fig. 2a). This indicates that satellite SSS with high spatial and temporal resolutions can capture more variability in the upper ocean, especially the high-frequency variability, without considering the observation errors.

The highest RMS value of SSS in the North Indian Ocean is mainly distributed in southeaste1630WeWern AS, region south of the Indian Peninsula and Sri Lanka, and along the coast of BoB. Among them, the SSS change along the coast of the BoB is the most distinctive, and the RMS peak value calculated using SMAP SSS is far more than 1.5 psu. The closer to the land, the greater the change in SSS, reflecting a strong influence from the land-sea interaction. In southeastern AS, the maximum RMS of SSS does not exist in the coastal area but has a high-value center in the open ocean with about 10° longitudinal distances from the west coast of India.

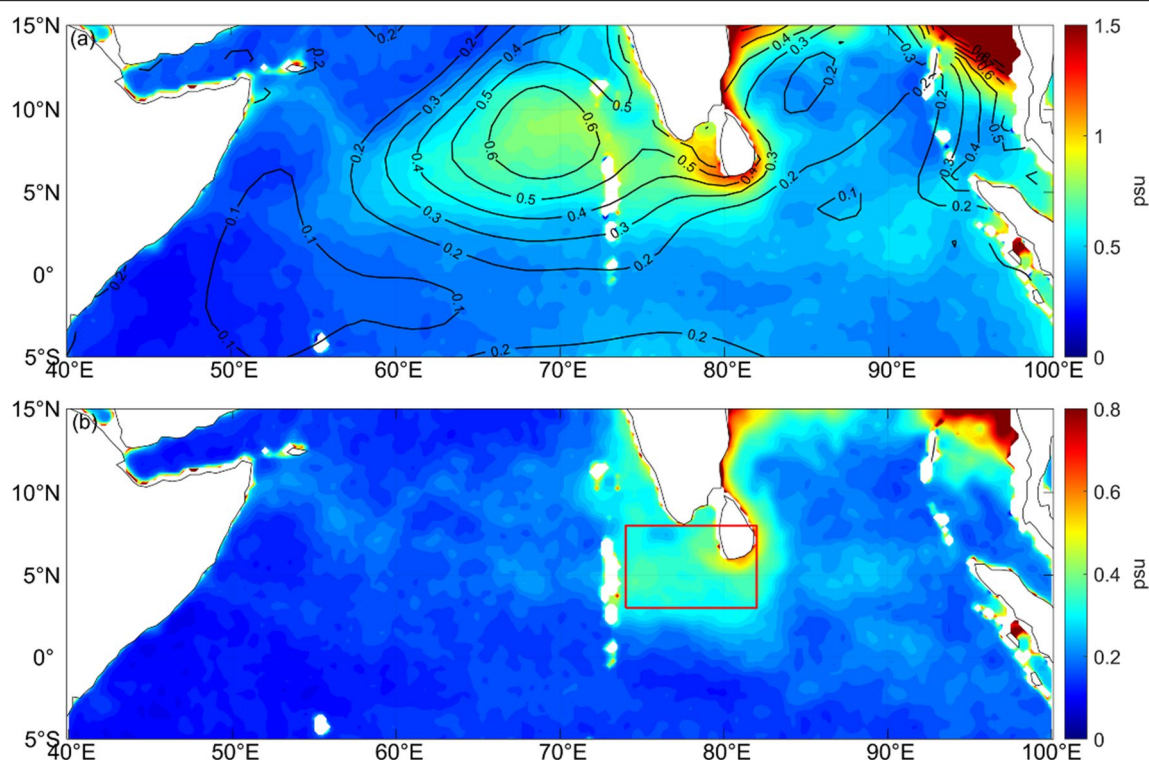The difference in the RMS between the climatological monthly mean and daily SSS is intense in the regions

Fig. 2 Root Mean Square of SSS (unit: psu) in the central and southern North Indian Ocean. **a** daily SMAP SSS (shading) and climatological WOA18 SSS (contour); **b** SMAP SSS filtered with a 30–120-day bandpass filter. The red box (74–82°E, 3–8°N) in b indicates the study area for Fig. 3

Zhu *et al. Geoscience Letters*   (2022) 9:37

Page 6 of 14

region south of the Indian Peninsula and Sri Lanka and along the coast of BoB, which is consistent with the RMS of the high-frequency SSS filtered with a band filter of 30–120 days (Fig. 2b). This further indicated that the satellite SSS captures the high-frequency variability of the SSS in these regions. Especially, the region south of the Indian Peninsula (74–82°E, 3–8°N) is the key channel for the water mass exchange between the AS and the BoB. Therefore, this study focuses on the change of SSS and related ocean dynamic processes in this region. Compared with the non-filtering result, the SSS variability is weakened, especially in southeastern AS, indicating that the SSS change in these regions is mainly caused by the mean current transport (Rao and Sivakumar 2002; Zhang and Du 2012).

In the region south of the Indian Peninsula, the climatological monthly mean and daily SSS have shown an apparent seasonal cycle in the past 4 years (Fig. 3a). The SSS is high in summer and fall but low in winter and spring. The lowest SSS appears in the late autumn and early winter (November to December). Then, it increases after April, and reaches the highest from July to October (Fig. 3a). The low-salinity water transported by the EICC and NMC from the northern BoB causes a sharply SSS decrease in November (Fig. 1d). Then, the freshwater caused by the Southwest Monsoon precipitation leads to the second decrease of the SSS from April to May. Later, with the development of the Southwest Monsoon, the SMC transports the high-salinity water from the AS into the region south of the Indian Peninsula, increasing the SSS there.

Compared to the SSS variability during spring and summer, the SSS changes in autumn and winter are more rapid and violent. In addition to the sharp decrease of SSS, a larger amplitude of oscillation occurs in the daily data than in the climatological monthly mean data (Fig. 3a). This indicates that the SSS experiences more pronounced intraseasonal variability in winter than in summer, which can be seen in the time series of the SSS filtered with a 30–120-day bandpass filter (Fig. 3b). Within less than 5 years, the low-SSS events in the autumn and winter of 2016 and 2017 are the most prominent and the weakest in 2019.

Intraseasonal variability of SSS was particularly significant in the autumn and winter of 2016, with amplitudes greater than 50% of the seasonal variation. This paper takes 2016 as a case to analyze the role of mesoscale eddies in the transport of low-salinity water during autumn and winter. Figure 4 shows the distribution of SSS and sea surface current anomalies, and SLA with 8-day intervals. The results show that on Oct 25, the low-salinity water along the west boundary of the BoB is transported southward to 12°N (Fig. 4a). Afterward, the low-salinity water tongue (31–31.5 psu) extended southward to the southeast coast of Sri Lanka at 5°N on November 2 due to the EICC transport (Fig. 4b). There are meridionally arranged eddies along the coasts of India and east of Sri Lanka during these periods. It is worth noting that a cyclonic eddy forms in the southeast corner of Sri Lanka and develops at the off-side of the coastal current (Fig. 4b). Eight days later, the NMC develops in the south of Sri Lanka and India. Meanwhile,
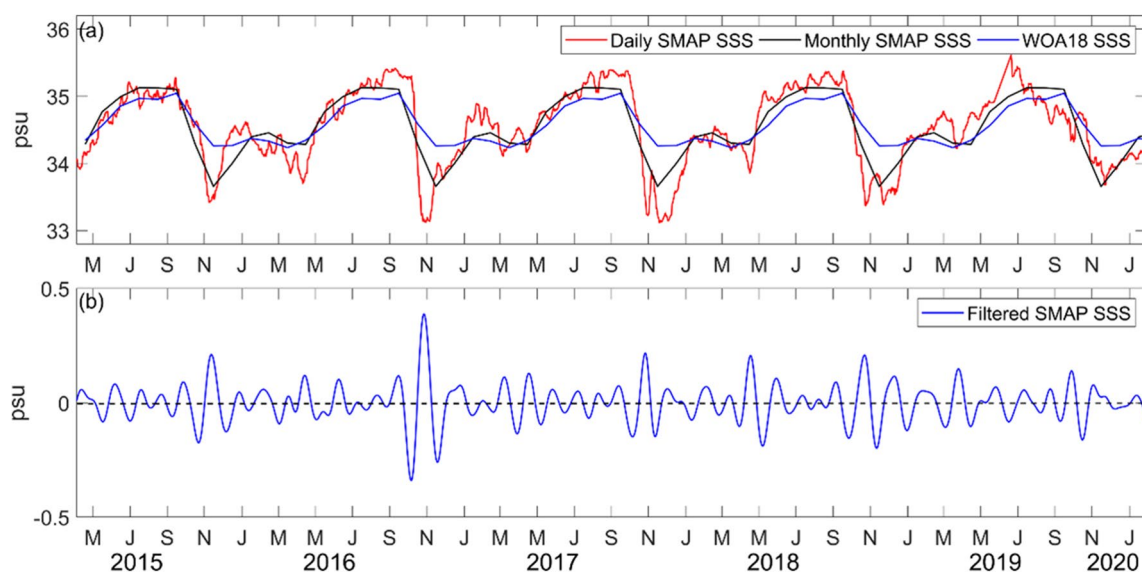

Fig. 3 Time series of regional mean SSS in the region south of the Indian Peninsula (74–82° E, 3–8° N). **a** Red curve is daily SMAP SSS, the black curve is monthly SMAP SSS, and the blue curve is climatology WOA18 SSS (**b**). The blue curve is filtered (30 ~ 60 days) SMAP SSS

Zhu *et al. Geoscience Letters* (2022) 9:37
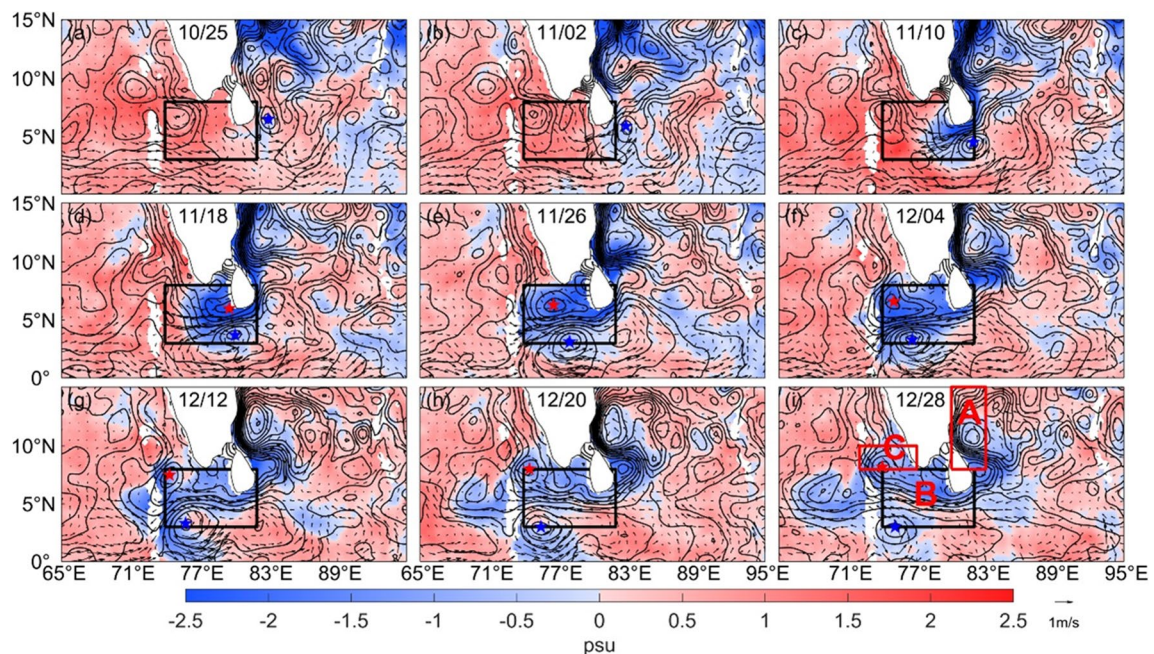
Page 7 of 14

Fig. 4 Distribution of SSS anomaly (shading; psu), SLA (contour; m), and sea surface current (vector; m/s) in autumn and winter 2016. The red star represents the core of the anticyclonic eddy, and the blue star represents the core of the cyclonic eddy. **A**, **B**, and **C** represent the location of the area in Figs. 6 and 7, respectively

the cyclonic eddy strengthens and transports westward along the south side of the NMC (Fig. 4c). Both the NMC and the cyclonic eddy help the westward transport of low-salinity water into the region south of the Indian Peninsula. On November 18, an anticyclonic eddy generates on the western side of Sri Lanka when the low-salinity water is transported to this region (Fig. 4d). The anticyclonic eddy develops quickly and transports westward along the north edge of the NMC. On November 26, an eddy pair forms in the region south of the Indian Peninsula with a cyclonic eddy south and an anticyclonic eddy north of the NMC (Fig. 4e). In this process, the eddy pair strengthened the westward transport of low-salinity water of the NMC. Later, the NMC and the eddy pair persists for nearly a month in the region south of the Indian Peninsula, blocked by the Maldivian terrain to the west. During this period, the NMC continues to transport the low-salinity water from the BoB to the region south of the Indian Peninsula, while the eddy pair plays an important role in redistributing the low-salinity transported to this region (Fig. 4e–h). By the end of December, the low-SSS water transported from the north BoB has been discontinued. At the same time, the eddy pair weakened, and the north anticyclonic transported northward, wrapping a large amount of the low-salinity water into the southeastern AS, forming the LH. LH did not deform until February (Shankar and Shetye 1997), and its

boundary jet continued to transport low-salinity water northward, providing low-salinity water for the coastal boundary jet. During the period after December 12, NMC flows westward across the Maldives island chain, and part of the low-salinity water leaked to the southern AS and extended westward.

In this low-salinity water event in late autumn and early winter, the SSS off southern India does not exhibit a simple continuous decrease in this process. Consequently, SSS in the region south of the Indian Peninsula and Sri Lanka appeared to have a large amplitude of intraseasonal variability.

To highlight the role of eddy in the transport of low-salinity water, two Argo floats (Float Nos.: 2901896 and 2,902,153) located near the low-salinity transport pathway during the event are analyzed in this study. Figure 5 shows the trajectory plots and salinity profiles for the two Argo floats from 20 October 2016 to 19 January 2017. The float No.2901896 was located along the eastern coast of Siri Lanka and moved southward during this period (Fig. 5a). Prior to the low-salinity water event, the SSS along the east coast of Sri Lanka was above 33 psu. On 31 October, low-salinity water transported by the EICC reached northeastern Sri Lanka, where salinity decreased dramatically to below 32 psu in the upper 40 m. This low value was maintained until mid-January of the following year (Fig. 5b).
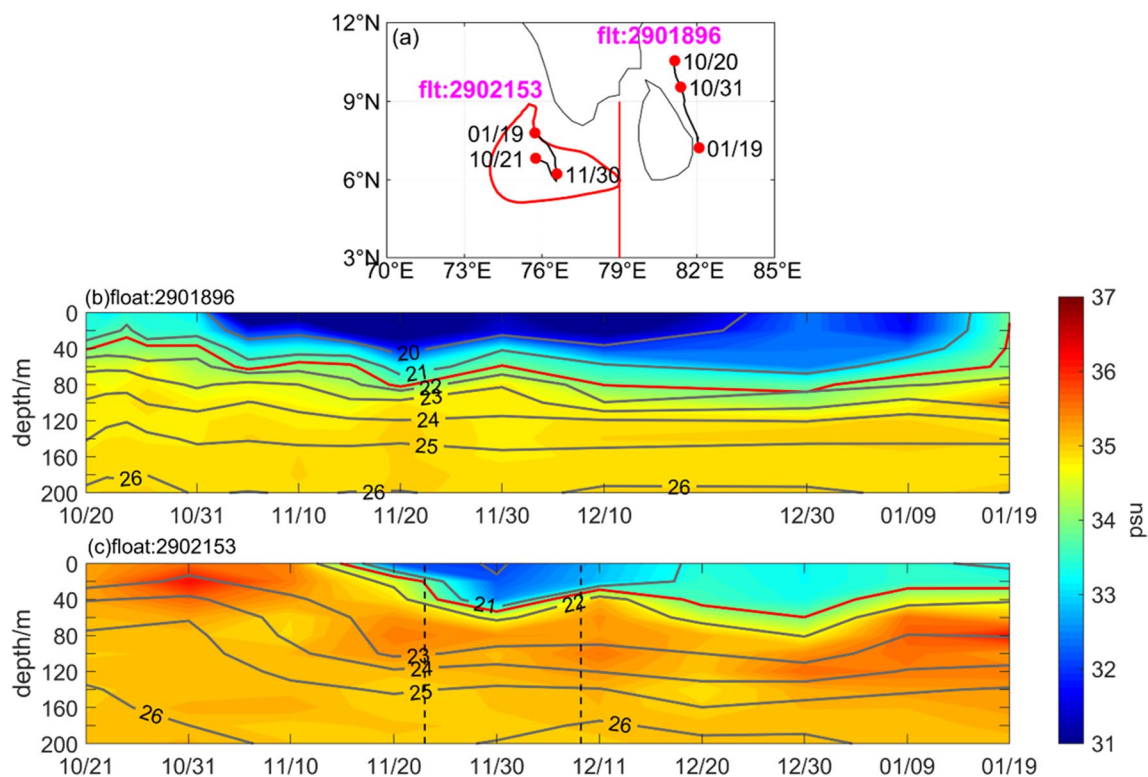
Fig.5 Trajectory maps (**a**) and salinity profile (**b**, **c**) from the two Argo floats from 20 October 2016 to 19 January 2017 as well as the anticyclonic eddy edge (**a**) on 30 November. The red line in **a** is the transect (79°E, 0–8°N). The gray contour lines represent the potential density and the red contour line represents the salinity of 33.9. Dashed lines represent the period when the Argo float is inside the eddy

Then, this low-salinity water was transported by the NMC through southeastern Sri Lanka and moved westward. On 15 November, the low-salinity water was captured by float No.2902153 in the region south of the Indian Peninsula. On 23 November, the float was located inside the anticyclonic eddy and remained there until 9 December. The water trapped in the anticyclone maintains a better low-salinity character, with salinity in the upper 50 m all below 33 psu, which is dramatically fresher than that outside of the anticyclone (Fig. 5c). The salinity in the upper 50 m was about 35 psu before the low-salinity water was transported to the region south of the Indian Peninsula, where its salinity dropped to nearly 33.5 psu outside the anticyclonic eddy after mixing with the low-salinity water transported from the northern BoB. Under the influence of low-salinity water, the halocline in the region south of the Indian Peninsula occurs near the isosaline line of 33.9 psu, which is near the mixed layer depth (Fig. 5c). The re-stratification of the upper layer water in southern India following the entry of low salinity water forms a new mixed layer with the depth near 50 m. Due to the homogeneous characteristics of the water within the mixed layer and the mixed layer depths in the region south of the Indian Peninsula

vary little with location, the SSS and the surface currents are used to calculate the relative contributions of eddy on the low-salinity water transport. The eddy low-salinity water volume transport is estimated by multiplying the area inside the eddy with sea surface salinity below 33.9 psu by the 50 m vertical depth. The total volume transport of low water through the 79°E transect was estimated by accumulating the volume fluxes through the transect during the low salinity event between 1 and 30 November. The volume fluxes is calculated by multiplying the zonal velocity with the corresponding area of low-salinity water on the transect within 50 m. The low-salinity water volume within the eddies accounted for 83% of the total volume transported through the transect, with anticyclonic eddies accounting for 67% and cyclonic eddies for 16%, when they moved away from the transect and reached maximum intensity on 30 November.

The above analysis suggests that low-salinity water transport from the northern BoB during winter significantly reduces the upper layer salinity in the region south of the Indian Peninsula. The anticyclonic eddy can maintain the low-salinity characteristics well and play an important role in low-salinity water transport between the AS and BoB.

Salinity budget analysis

Through the salinity budget equation, we further verify the dominant process of salinity change in this region. The result shows that the contribution of local freshwater flux is relatively small. The horizontal advection term is consistent with the change of salinity and the transport of high- and low-salinity water by sea surface current is the main reason for the local change of SSS (Fig. 6a).

Consistent with the above analysis, the SSS decreases sharply during late autumn and early winter and increases during the summer monsoon each year caused by the horizontal salinity transport (Fig. 6b, c). However, the process of rebound increase in SSS appears because of the weakening of low-salinity water transport, showing obvious intraseasonal variability characteristics (Fig. 6a). Different from autumn and winter, the amplitude of salinity change in summer is small. Most of the
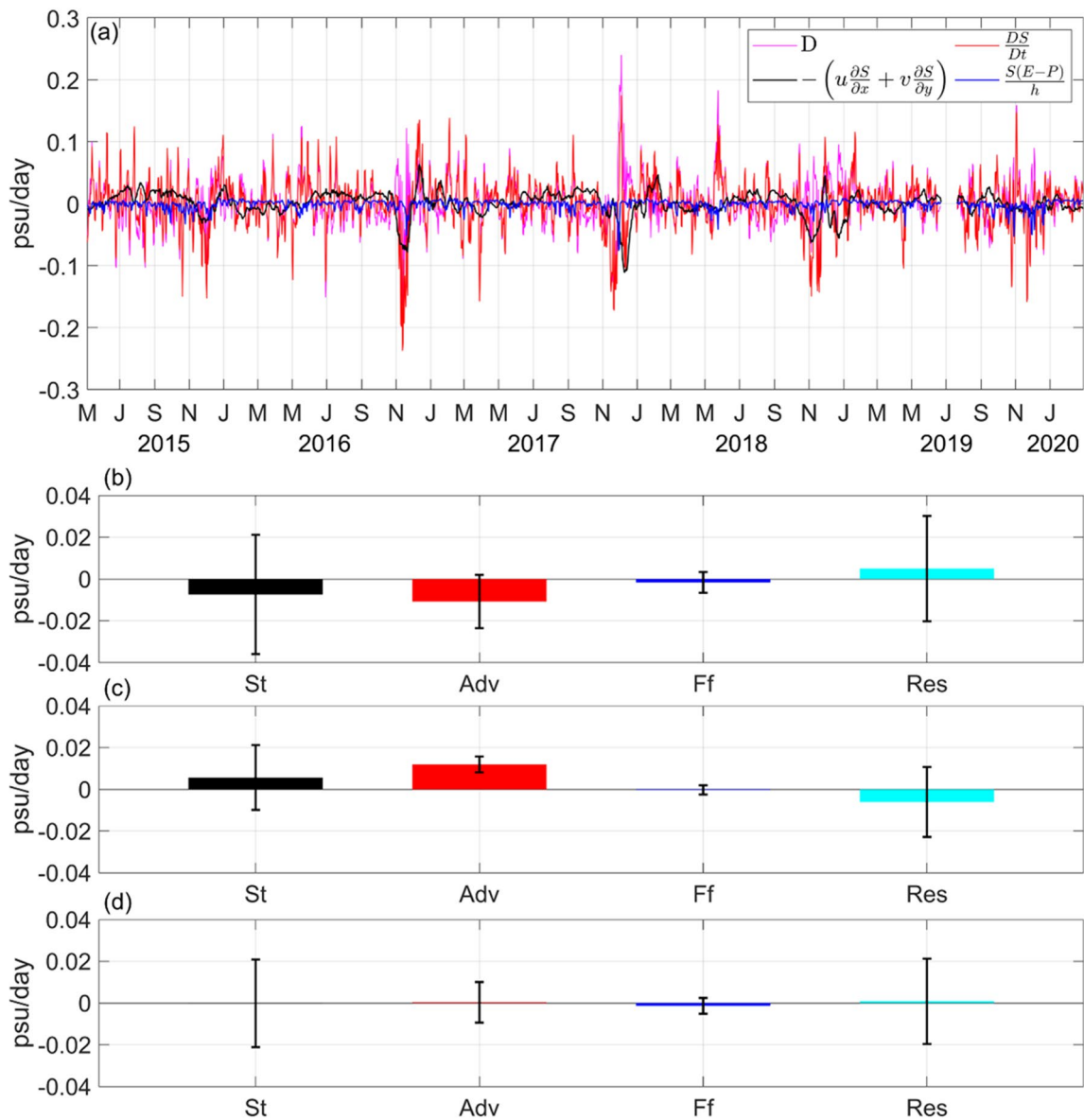

Fig. 6 a Time series of salinity budget equation in region B (74°–82°E, 3–8°N) during 2015–2019. **b** Wintertime mean salinity budget terms (bars, psu/day) and the half of the standard error. **c** Summertime mean salinity budget terms (bars, psu/day) and the half of the standard error. **d** Five-year mean salinity budget terms (psu/day) and the half of standard error. St represents the salinity tendency, Ff represents the freshwater flux term, and Adv represents the horizontal advection terms. Res represents the residual term calculated by (St-Adv-Ff)

SSS increase is also caused by positive high-salinity water transport (Fig. 6c). From May to September, stable SMC transported high-salinity waters from the AS to the BoB, flowing through the region south of the Indian Peninsula, increasing SSS there. For the 5-year mean, the SSS is balanced by winter and summer low- and high-salinity water exchange (Fig. 6d). Note that the residual term, which includes the errors of the observations, and the effects of vertical entrainment, diffusion, mixing, is quite large. This is mainly caused by errors in the observations. These observations have different spatial and temporal resolutions, which can produce significant errors in the calculation of salinity budgets due to mismatches in the data properties. The large standard errors, especially in winter, indicate a strong effect of high-frequency variability.

Influenced by the eddy pair, the process of low-salinity water transport during the autumn and winter of 2016 showed significant intraseasonal variability. To further clarify the contribution of high-frequency processes, we decompose the advection term into three parts as

$$-\left[\left(\bar{u}\frac{\partial \bar{S}}{\partial x}+\bar{v}\frac{\partial \bar{S}}{\partial y}\right)+\left(\bar{u}\frac{\partial S'}{\partial x}+\bar{v}\frac{\partial S'}{\partial y}+u'\frac{\partial \bar{S}}{\partial x}+v'\frac{\partial \bar{S}}{\partial y}\right)+\left(u'\frac{\partial S'}{\partial x}+v'\frac{\partial S'}{\partial y}\right)\right]$$

These three terms represent the contributions of the seasonal mean processes, current perturbation associated with eddy and the salinity gradient disturbance caused by jet transport, and the non-linear high-frequency disturbances, respectively. Along the pathway of the low-salinity water outflow, the latter two terms can represent the influence of eddy, high-frequency jets, and their interactions. Figure 7 shows the time series of each component of the horizontal advection term in the eastern boundary region of India and Sri Lanka (region A, 80°–83°E, 8°–15°N), the region south of Sri Lanka and India (region B, 74°–82°E, 3–8°N) and the western boundary region of India (region C, 72°–77°E, 8°–10°N) from September 2016 to February 2017.

The results show that from late October, the amplitude of the horizontal advection in region A increases significantly (Fig. 7a). In addition to the mean term $\left(-\left(\bar{u}\frac{\partial \bar{S}}{\partial x}+\bar{v}\frac{\partial \bar{S}}{\partial y}\right)\right)$, other perturbation terms including the mean flow and perturbation of SSS gradient interaction term $\left(-\left(\bar{u}\frac{\partial S'}{\partial x}+\bar{v}\frac{\partial S'}{\partial y}\right)\right)$, perturbation of flow and mean SSS gradient interaction term $\left(-\left(u'\frac{\partial \bar{S}}{\partial x}+v'\frac{\partial \bar{S}}{\partial y}\right)\right)$ and perturbation of flow and SSS gradient interaction term $\left(-\left(u'\frac{\partial S'}{\partial x}+v'\frac{\partial S'}{\partial y}\right)\right)$ contribute to the decrease of SSS as well. Among them, affected by the eddy and the perturbation of low-salinity water transport in the north, the perturbation of flow and SSS gradient interaction term makes the most significant contribution to the SSS change in the eastern boundary of India and Sri Lanka (Fig. 7a). The process lasted until mid-December, with a peak at the end of October and early December, respectively. In terms of the later peak, the effect of perturbation of flow and SSS gradient interaction term is equivalent to that of mean flow and perturbation of SSS gradient interaction term, which jointly leads to the decrease of SSS (Fig. 7a). In other months, the horizontal advection had little change.

In region B, the rapid increase of negative horizontal advection occurs in early November, which is about 10-day lag in region A (Fig. 7b). This indicates that it takes about 10 days for the negative signal to propagate from region A to region B. The low-salinity event in region B lasts about a month. In the first 20 days, the mean flow and perturbation of the SSS gradient interaction term and the perturbation of flow and mean SSS gradient interaction term both contribute to the negative horizontal advection. The latter accounts for a larger proportion in the first half month, reflecting the influence of the eddy propagating on local SSS. In late November, EICC begins to weaken, and the mean flow and perturbation of the SSS gradient interaction term also weaken. At the same time, as the cyclonic eddy encounters the Maldives island chain, the moving speed slows down. The entrainment of the local cyclonic eddy on the surrounding high-SSS water makes the perturbation of flow and perturbation of SSS gradient interaction term transfers to positive values. The cyclonic eddy gradually weakens under the influence of topography. On one hand, the decrease of EICC leads to the decrease of low-salinity water volume from the BoB to region B, while the NMC imports the relatively high-SSS water from the southern BoB to the west of the region B. On the other hand, as the eddy pair slowly moves out of region B, the NMC in the west of region B tends to be stable, and the velocity decreases. The mean flow and perturbation of the SSS gradient interaction term dominate the change of subsequent horizontal advection, and the positive horizontal advection peaks in early December and mid-January, respectively.

The influence of low-salinity waters on the southeast AS (region C) lags far behind that of region B for about 1 month. The regional SSS has continued to decrease since the beginning of December, and it has weakened significantly until the beginning of January. The negative advection generated by the mean flow
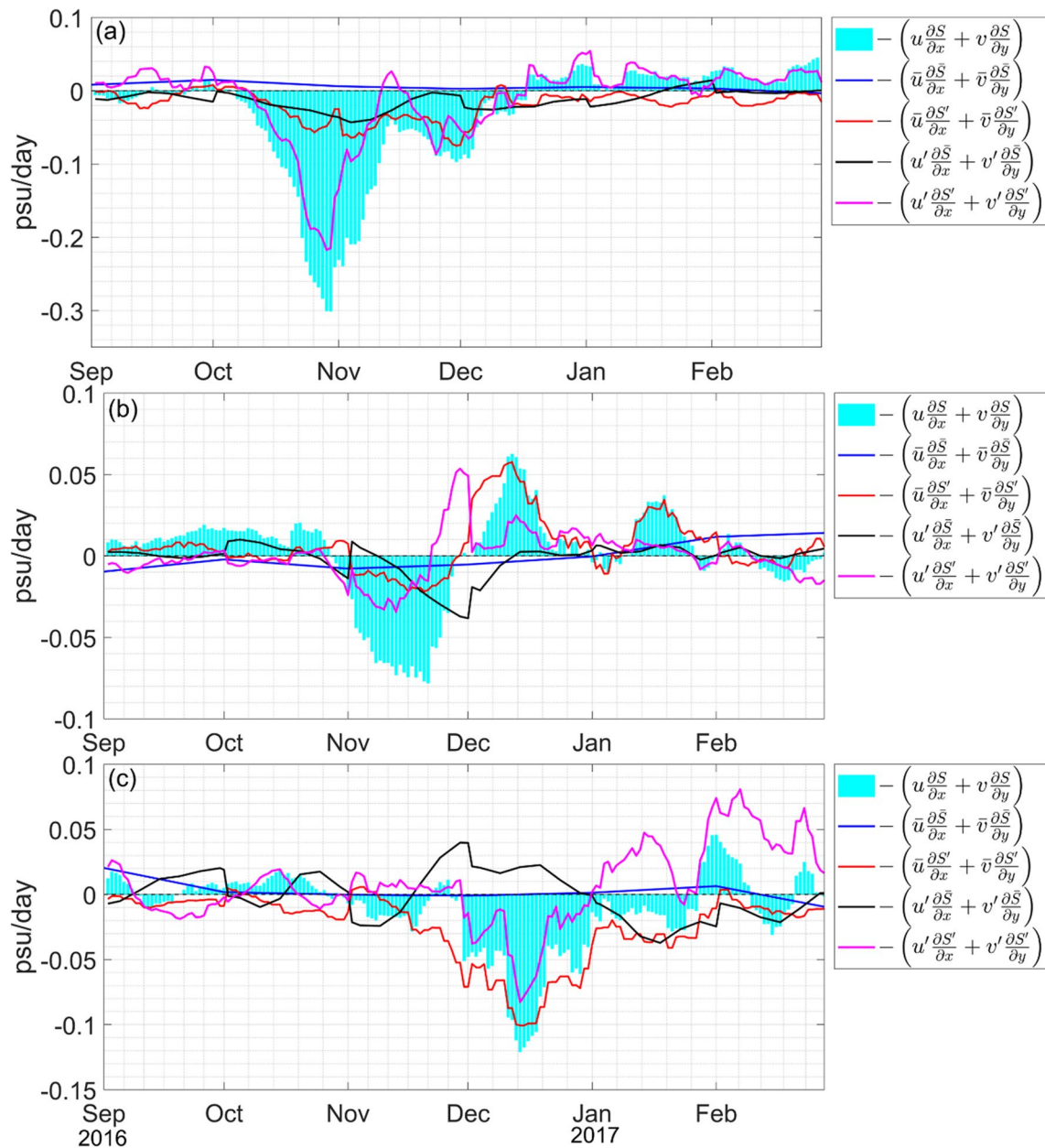
Fig. 7 Time series of components of horizontal advection in three regions along the pathway of the low-salinity water transport from September 2016 to February 2017. **a** Region A (80°–83°E, 8°–15°N); **b** Region B (74°–82°E, 3°–8°N); **c** Region C (72°–77°E, 8°–10°N)

and perturbation of the SSS gradient interaction term continues throughout the winter from November. The perturbation of flow and SSS gradient interaction term only causes local salinity to decrease within December, and changes from negative to positive after January. During this period, the perturbation of flow and mean salinity gradient interaction term are just opposite to the perturbation of flow and SSS gradient interaction terms, indicating that a large amount of low-salinity

water is transported northward at the western edge of the anticyclonic eddy, resulting in SSS gradient opposite to the mean west–north decrease (Fig. 4f–i). The two terms offset each other, contributing little to the horizontal advection term in region C. The SSS decline is mainly dominated by the mean flow and perturbation of the SSS gradient interaction term. The analysis of region C indicated that LH can cause SSS disturbance in the southeast AS, but have little influence on the

Zhu *et al. Geoscience Letters*   (2022) 9:37

Page 12 of 14

northward transport of low-salinity water. The northward mean flow along the coast dominates the northward transport of low-salinity water (Fig. 4i).

Overall, the horizontal advection in region A is the strongest among the three regions. In addition, the perturbation of flow caused by EICC and the related eddies and their southward low-salinity water transport dominate the low-salinity event from late October to early November. Since the direction of the flow perturbation and the SSS gradient are consistent with the mean state, the three disturbing terms all contribute to low-salinity water events. The low-salinity water in region A was transported to region B after 10 days under the combined influence of three perturbations. The eddy pair in region B together with the mean flow transports the low-salinity water westward. Due to the blocking of the Maldives island chain, the eddy pair transports slowly. Consequently, the low-salinity water in region B does not enter region C until 1 month later. The low-salinity water event in region C is dominated by the transport of mean flow, since the influence of the perturbation terms associated with eddy is weakened by offsetting each other. This further indicates that the intraseasonal variation of SSS in the region south of the Indian Peninsula is not only caused by the transport of local eddy, but also the salinity gradient caused by the coastal jet low-salinity transport.

Summary and discussion
Summary
The monsoon heavily influences the North Indian Ocean. The sea surface current system is complex, and the temporal and spatial differences in evaporation and precipitation are notable. There is abundant precipitation over BoB during Southwest Monsoon, and many large rivers of South Asia flow into the northern BoB. In comparison, the evaporation exceeds the precipitation in the AS throughout the year. As a result, a large gradient of the SSS appears in the northern Indian Ocean, with the basin difference larger than 3 psu. To balance the SSS caused by the freshwater flux, the seasonally reversed current plays an important role in high- and low-SSS exchange between AS and BoB. During the Southwest Monsoon, the clockwise circulation forms in the northern Indian Ocean, in which a strong eastward SMC occurs in the region south of the Indian Peninsula, transporting high-salinity water from the AS into the southcentral BoB. In winter, low-salinity waters from the northern BoB were transported southward by EICC to the eastern side of Sri Lanka and then advected westward to the AS by NMC.

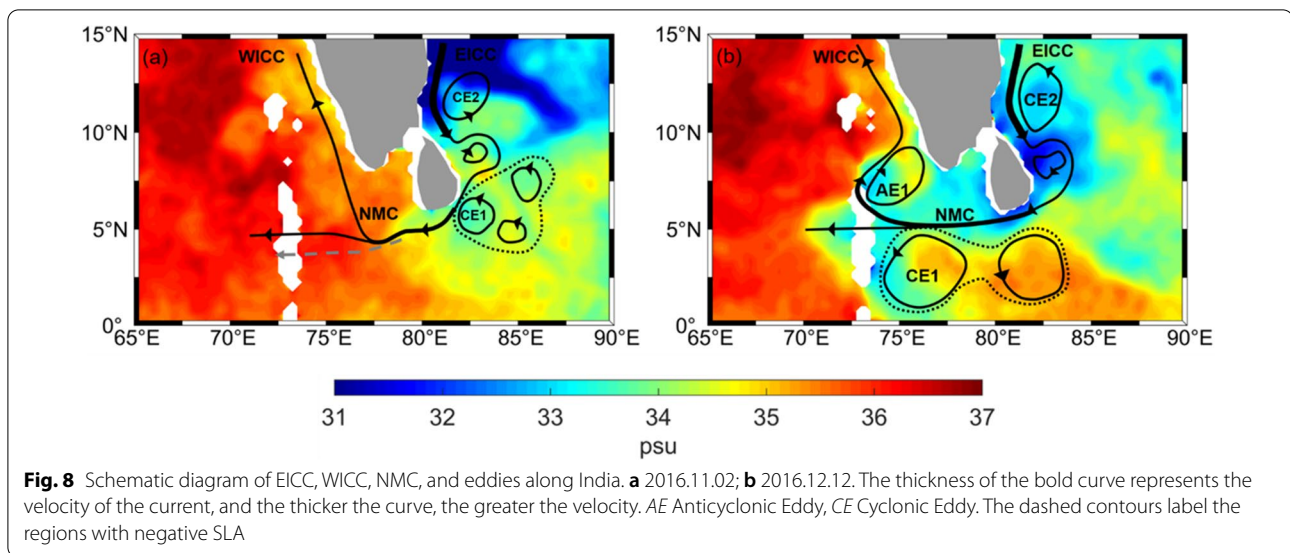The region south of the Indian Peninsula is a key area for water mass exchange between the two basins. The analysis of satellite SSS shows that significant intraseasonal variability of SSS occurs in the region south of the Indian Peninsula, especially in late autumn and early winter. Further analysis indicates that the most significant SSS decreases occurred in late autumn and winter of 2016. Meanwhile, an eddy pair developed in the region south of the Indian Peninsula, favoring the transport of low-salinity water and the SSS intraseasonal variability.

Based on the salinity budget analysis in the regions, including the eastern coast of India, the region south of the Indian Peninsula, and the western coast of India, along the pathway of low-salinity water transport, the eddy's role in the regional SSS variability is investigated. In the eastern coastal region of India, EICC and its related eddies dominate the low-salinity water transport and the regional intraseasonal variability of the SSS (Fig. 8a). In the region south of the Indian Peninsula, an eddy pair develops with the NMC with the cyclonic south and the anticyclonic north of the main flow for more than 1 month, transporting the low-SSS water into this region and enhancing the intraseasonal variability of SSS (Fig. 8b). The energy for the development and growth of the CE1 comes not only from the instability of jets, but also from the interior ocean planetary waves. The negative SLA forms a gyre south of the jets and several other eddies within it. During the winter of 2016, the eddies contribute to the growth and maintenance of the CE1 by merging them into CE1. In addition, the propagation of positive SLA signal contributes to the generation of AE1 in the west of Sri Lanka. The anticyclonic and the edge-jet bring the low-salinity water transported from the northern BoB northward into southeastern AS, contributing to the SSS decrease there. The cyclonic eddy weakens at the east of the Maldives island chain due to the blocking of the topography.

Discussion
This paper analyzes the influence of an eddy pair on the low-salinity water transport from the BoB to the AS during late autumn and earlier winter in 2016. The results show that significant intraseasonal variability of SSS occurs along the pathway of the low-salinity water transport, and the coastal jets and the eddies contribute to most of it. The conditions in the other years also show the important role of the eddy, but with different strengths and patterns. In the autumn and winter of 2017, there was an anticyclonic eddy propagating from southeast Sri Lanka to the southeast Arabian Sea, while no cyclonic eddy was generated. The generation and extinction time of eddy pairs in other years are also different.

The western coast of the BoB is a key area of eddy-current interaction (Chen et al. 2012). Some studies

Zhu *et al. Geoscience Letters* (2022) 9:37

Page 13 of 14

Fig. 8 Schematic diagram of EICC, WICC, NMC, and eddies along India. **a** 2016.11.02; **b** 2016.12.12. The thickness of the bold curve represents the velocity of the current, and the thicker the curve, the greater the velocity. *AE* Anticyclonic Eddy, *CE* Cyclonic Eddy. The dashed contours label the regions with negative SLA

have been conducted on the dynamical mechanism of EICC and coastal eddies. Yu et al. (1991) suggested that the remote forcing from the equator drove the semiannual reverse of the upper ocean circulation in the BoB. Model results (Sen et al. 2022) revealed that wind stress curl plays an important role in the semiannual reverse of EICC. The remote forcing modulated by equatorial wind anomaly dominates the southward transport of EICC.

In addition, the temporal resolution of the sea surface current field is 5 days, while the temporal resolution of sea surface salinity is daily (8-day moving average). It can be seen that horizontal advection plays an important role in SSS change, but it cannot fully explain the higher frequency of SSS variability. This also indicates that geostrophic current based on the inversion of sea surface height observation cannot meet the research needs of high-frequency salinity change and cannot estimate the regional salinity balance well.

Abbreviations
AS: Arabian Sea; BoB: Bay of Bengal; C3S: Copernicus Climate Change Service; ECMWF: European Centre for Medium-Range Weather Forecasts; EICC: East Indian Coastal Current; ISO: Intraseasonal Oscillation; ISV: Intraseasonal Variability; JPL: Jet Propulsion Laboratory; LH: Lakshadweep high; MJO: Madden–Julian Oscillation; NASA: National Aeronautics and Space Administration; NCEI: National Oceanographic Data Center; NMC: Northeast monsoon current; OSCAR: Ocean surface current analysis real-time; SLA: Sea level anomaly; SMAP: Soil moisture active passive; SMC: Southwest Monsoon Current; SMOS: Soil Moisture and Ocean Salinity; SSS: Sea surface salinity; WDS: World Data Service; WOA18: World Ocean Atlas 2018.

Author contributions
All authors provided comments on different versions of the paper. All authors read and approved the final manuscript.

Availability of data and materials
The JPL SMAP Level 3 CAP Sea Surface Salinity Standard Mapped Image 8-Day Running Mean V5.0 Validated Data set is accessible from https://poda-ac.jpl. nasa.gov/dataset/SMAP_JPL_L3_SSS_CAP_8DAY-RUNNINGMEAN_V5. The World Ocean Atlas 2018 data set is accessible from https://www.ncei.noaa. gov/access/metadata/landing-page/bin/iso?id=gov.noaa.nodc:NCEI-WOA18. The Argo profile data is accessible from http://www.argodatamgt.org/Access-to-data/Argo-data-selection. The ocean surface currents data set is accessible from http://podaac.jpl.nasa.gov/dataset/OSCA-R_L4_OC_third-deg. The Sea level data set is accessible from https://cds.climate.copernicus.eu/cdsapp#!/dataset/satellite-sea-level-global?tab=form. The evaporation and precipitation data set is accessible from https://cds.climate.copernicus.eu/cdsapp#!/software/app-c3s-daily-era5-statistics?tab=app.

Declarations

Ethics approval and consent to participate
Not applicable.

Consent for publication
Not applicable.

Competing interests
The authors have no competing interests.

Author details
[1]State Key Laboratory of Tropical Oceanography, South China Sea Institute of Oceanology, Chinese Academy of Sciences, Guangzhou 510301, China. [2]College of Marine Science, University of Chinese Academy of Sciences, Beijing 100049, China. [3]Southern Marine Science and Engineering Guangdong Laboratory (Guangzhou), Guangzhou 511458, China. [4]College of Oceanography, Hohai University, Nanjing 210098, China.

References

Babu MT, Kumar PS, Rao DP (1991) A subsurface cyclonic eddy in the Bay of Bengal. J Mar Res 49(3):403–410. https://doi.org/10.1357/002224091784995846

Bonjean F, Lagerloef GSE (2002) Diagnostic model and analysis of the surface currents in the tropical Pacific Ocean. J Phys Oceanogr 32:2938–2954. https://doi.org/10.1175/1520-0485(2002)032%3c2938:DMAAOT%3e2.0.CO;2

Bruce JG, Johnson GDR, Kindle JC (1994) Evidence for eddy formation in the eastern Arabian Sea during the northeast monsoon. J Geophys Res 99(14):7–651. https://doi.org/10.1029/94JC00035

Chen G, Wang D, Hou Y (2012) The features and interannual variability mechanism of mesoscale eddies in the Bay of Bengal. Cont Shelf Res 47:178–185. https://doi.org/10.1016/j.csr.2012.07.011

Cheng X, McCreary JP, Qiu B, Qi Y, Du Y (2017) Intraseasonal-to-semiannual variability of sea-surface height in the astern, equatorial Indian Ocean and southern Bay of Bengal. J Geophys Res 122(5):4051–4067. https://doi.org/10.1002/2016JC012662

Durack PJ, Wijffels SE, Matear RJ (2012) Ocean salinities reveal strong global water cycle intensification during 1950 to 2000. Science 336(6080):455–458. https://doi.org/10.1126/science.1212222

Durand F, Shankar D, de Boyer MC, Shenoi SSC, Blanke B, Madec G (2007) Modeling the barrier-layer formation in the Southeastern Arabian Sea. J Clim 20:2109–2120. https://doi.org/10.1175/JCLI4112.1

Durand F, Shankar D, Birol F, Shenoi SSC (2009) Spatiotemporal structure of the East India Coastal Current from satellite altimetry. J Geophys Res 114:C02013. https://doi.org/10.1029/2008JC004807

Fore AG, Yueh SH, Tang W, Stiles BW, Hayashi AK (2016) Combined Active/Passive Retrievals of Ocean Vector Wind and Sea Surface Salinity With SMAP. IEEE Trans Geosci Remote Sens 54(12):7396–7404

Garcia HE, Boyer TP, Baranova OK, Locarnini PA, Mishonov AV, Grodsky A, Paver CR, Weathers KW, Smolyar IV, Reagan JR, Seidov D, Zweng MM (2019) World

Greaser SR, Subrahmanyam B, Trott CB, Roman-Stork HL (2020) Interactions Between Mesoscale Eddies and Synoptic Oscillations in the Bay of Bengal During the Strong Monsoon of 2019. J Geophys Res 125:10. https://doi.org/10.1029/2020JC016772

Han W, McCreary JP (2001) Modeling salinity distribution in the Indian Ocean. J Geophys Res 106(C1):859–877. https://doi.org/10.1029/2000JC000316

Hasson A, Farrar JT, Boutin J, Bingham F, Lee T (2019) Intraseasonal Variability of Surface Salinity in the Eastern Tropical Pacific Associated with Mesoscale Eddies. J Geophys Res 124(4):2861–2875. https://doi.org/10.1029/2018JC014175

Hormanna V, Centurionia LR, Gordonb AL (2019) Freshwater export pathways from the Bay of Bengal. Deep Sea Res Part II 168:104645. https://doi.org/10.1016/j.dsr2.2019.104645

Howden SD, Murtugudde R (2001) Effects of river inputs into the Bay of Bengal. J Geophys Res 106(C9):19825–19843. https://doi.org/10.1029/2000JC000656

Kohler J, Serra N, Bryan FO, Johnson BK, Stammer D (2018) Mechanisms of mixed-layer salinity seasonal variability in the Indian Ocean. J Geophys Res 123:466–496. https://doi.org/10.1002/2017JC013640

Kurian J, Vinayachandran PN (2007) Mechanisms of formation of the Arabian Sea mini warm pool in a high-resolution Ocean General Circulation Model. J Geophys Res 112(C5):C05009. https://doi.org/10.1029/2006JC003631

Murtugudde R, Busalacchi AJ (1998) Salinity effects in a tropical ocean model. J Geophys Res 103(C2):3283–3300. https://doi.org/10.1029/97JC02438

Nyadjro ES, Subrahmanyam B, Murty VSN, Shriver JF (2012) The role of salinity on the dynamics of the Arabian Sea mini warm pool. J Geophys Res 117:9. https://doi.org/10.1029/2012jc007978

Ocean Atlas 2018: Product Documentation. A. Mishonov, Technical Editor.

Qu T, Lian Z, Nie X, Wei Z (2019) Eddy-induced meridional salt flux and its impacts on the sea surface salinity maxima in the southern subtropical oceans. Geophys Res Lett. https://doi.org/10.1029/2019GL084807

Rao RR, Sivakumar R (2002) Seasonal variability of sea surface salinity and salt budget of the mixed layer of the north Indian Ocean. J Geophys Res 108(C1):3009–3022. https://doi.org/10.1029/2001JC00907

Rao RR, Sivakumar R (2003) Seasonal variability of sea surface salinity and salt budget of the mixed layer of the north Indian Ocean. J Geophys Res 108(C1):9–1. https://doi.org/10.1029/2001jc000907

Schott FA, McCreary JP (2001) The monsoon circulation of the Indian Ocean. Prog Oceanogr 51(1):1–123. https://doi.org/10.1016/S0079-6611(01)00083-0

Schott FA, Xie SP, McCreary JP Jr (2009) Indian Ocean circulation and climate variability. Rev Geophys 47(1):1002

Schott FA, Xie SP, McCreary JP (2009) Indian Ocean circulation and climate

Sen R, Pandey S, Dandapat S, Francis PA, Chakraborty A (2022) A numerical study on seasonal transport variability of the North Indian Ocean boundary currents using Regional Ocean Modeling System (ROMS). J Oper Oceanogr 15(1):32–51

Shankar D, Shetye SR (1997) On the dynamics of the Lakshadweep high and low in the southeastern Arabian Sea. J Geophys Res 102(C6):12551–12562. https://doi.org/10.1029/97JC00465

Shankar D, Vinayachandran PN, Unnikrishnan AS (2002) The monsoon currents in the north Indian Ocean. Progr Oceanogr. 52(1):63–120. https://doi.org/10.1016/S0079-6611(02)00024-1

Shenoi SSC, Shankar D, Michael GS, Kurian J, Varma KK, Ramesh Kumar MR, Almeida Unnikrishnan AS, Fernandes W, Barreto N, Gnanaseelan C, Mathew R, Praju KV, Mahale V (2005) Hydrography and water masses in the southeastern Arabian Sea during March–June 2003. J Earth Syst Sci 114:475–491. https://doi.org/10.1007/BF02702024

Shetye SR, Gouveia AD, Shankar D, Shenoi SSC, Vinayachandran PN, Sundar D, Michael GS, Nampoothiri G (1996) Hydrography and circulation in the western Bay of Bengal during the northeast monsoon. J Geophys Res 101:14011–14025. https://doi.org/10.1029/95JC03307

Srivastava A, Gera A, Momin IM (2020) The impact of northern Indian Ocean rivers on the Bay of Bengal using NEMO global ocean model. Acta Oceanol Sin 39:45–55. https://doi.org/10.1007/s13131-020-1537-9

Subrahmanyam B, Roman-Stork HL, Murty VSN (2020) Response of the Bay of Bengal to 3–7-Day Synoptic Oscillations During the Southwest Monsoon of 2019. J Geophys Res 125:6. https://doi.org/10.1029/2020JC016200

Vinayachandran PN, Murty VSN, Ramesh Babu V (2002) Observation of barrier layer formation in the Bay of Bengal during summer monsoon. J Geophys Res 107(C12):8018–8026. https://doi.org/10.1029/2001JC000831

Vinayachandran PN, Kagimoto T, Masumoto Y, Chauhan P, Nayak SR, Yamagata T (2005) Bifurcation of the East India Coastal Current east of Sri Lanka. Geophys Res Lett 32(15):L15606. https://doi.org/10.1029/2005GL022864

Vinogradova N, Lee T, Boutin J, Drushka K, Fournier S, Sabia R, Stammer D, Bayler E, Reul N, Gordon A, Melnichenko O, Li L, Hackert E, Martin M, Kolodziejczyk N, Hasson A, Brown S, Misra S, Lindstrom E (2019) Satellite Salinity Observing System: Recent Discoveries and the Way Forward. Front Mar Sci 6(243):1–23

Yu Z, McCreary JP (2004) Assessing precipitation products in the Indian Ocean using an ocean model. J Geophys Res 109(C5):C05013

Yu L, O'Brien JJ, Yang J (1991) On the Remote Forcing of the Circulation in the Bay of Bengal. J Geophys Res 96(C11):20449–20454. https://doi.org/10.1029/91JC02424

Zhang YH, Du Y (2012) Seasonal variability of salinity budget and water exchange in the northern Indian Ocean from HYCOM assimilation. Chin J Oceanol Limnol 30(6):1082–1092. https://doi.org/10.1007/s00343-012-1284-7

Zhang YH, Du Y, JAYARATHNA WNDS, Sun QW, Zhang Y, Yao FC, Feng M, (2020) A Prolonged High-Salinity Event in the Northern Arabian Sea during 2014–17. J Phys Oceanogr 50(4):849–865. https://doi.org/10.1175/JPO-D-19-0220.1